Deposition of Cellulose Nanocrystals onto Supported Lipid Membranes

Yotam Navon, Bruno Jean, Liliane Coche-Guérente, Franck Dahlem, Anne Bernheim-Groswasser, Laurent Heux

LANGMUIR

Interface Components: Nanoparticles, Colloids, Emulsions, Surfactants, Proteins, Polymers

Deposition of cellulose nanocrystals onto biomimetic lipid membranes

Yotam Navon, Bruno Jean, Liliane Coche-Guerente, Franck Dahlem, Anne Bernheim-Groswasser, and Laurent Heux

Langmuir, **Just Accepted Manuscript** • DOI: 10.1021/acs.langmuir.9b02888 • Publication Date (Web): 06 Jan 2020

Deposition of cellulose nanocrystals onto biomimetic lipid membranes

*Yotam Navon,[a,b] Bruno Jean,[a] Liliane Coche-Guérente,[c] Franck Dahlem,[a] Anne Bernheim-Groswasser[*b] and Laurent Heux [*a]*

[a]Univ. Grenoble Alpes, CNRS, CERMAV, 38000 Grenoble, France.

[b]Department of Chemical Engineering, Ilse Kats Institute for Nanoscale Science and Technology, Ben Gurion University of the Negev, Beer-Sheva 84105, Israel.

[c]University of Grenoble Alpes, DCM UMR 5250, F-38000, Grenoble, France.

KEYWORDS: Supported lipid bilayers, Cellulose nanocrystals, Quartz crystal microbalance with dissipation monitoring, Scanning force microscopy, Total internal reflection fluorescence microscopy, Bioinspired thin films.

ABSTRACT

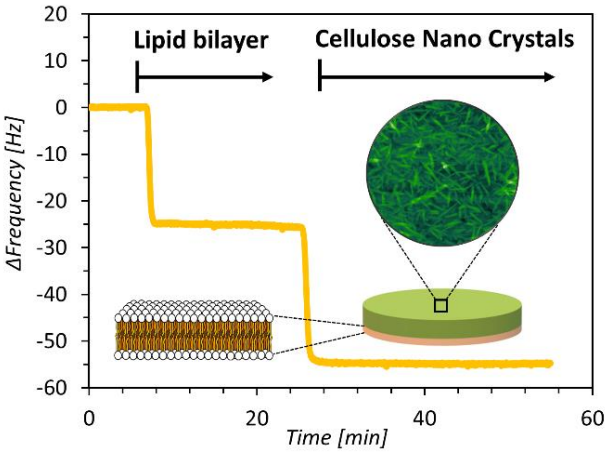

The deposition of cellulose nanocrystals (CNCs) on a supported lipid bilayer (SLB) was investigated at different length scales. Quartz crystal microbalance with dissipation monitoring (QCM-D) was used to probe the bilayer formation and to show for the first time the CNCs deposition onto the SLB. Specifically, classical QCM-D measurements gave estimation of the adsorbed hydrated mass and the corresponding film thickness, whereas complementary experiments using D_2O as the solvent allowed the quantitative determination of the hydration of the CNCs layer, showing a high hydration value. Scanning force microscopy (SFM) and total internal reflection fluorescence microscopy (TIRF) were used to probe the homogeneity of the deposited layers and reveal the structural details at the particle and film length scales, respectively, and to give information on the effect of CNCs concentration on the surface coverage. The results showed that the adsorption of CNCs on the supported lipid membrane depends on lipid composition, CNCs concentration and pH conditions, and that the binding process was governed by electrostatic interactions. Under suitable conditions, a uniform film was formed, with thickness corresponding to a CNCs monolayer, which provides the basis for a relevant 2D model of primary plant cell wall.

Introduction

The interaction of model lipid membranes and nanoparticles or biopolymers is a widely studied subject that has been investigated in numerous situations, for example to obtain information on the

toxicity of nanomaterials[1], to help for the rational design of liposomal drug delivery systems[2], or to study various biological processes, detached from the complexity of living cells.[3, 4] Nanoparticles can interact with lipid membranes either by adsorbing on the surface or *via* insertion into the bilayer, depending on the nature of the interacting components. It has been shown that several characteristics may influence the way nanoparticles interact with the membrane such as nanoparticle hydrophobicity,[5] surface charge[6, 7] and nanoparticle size.[8]

Various characterization techniques can be used to investigate the structural details of the interaction of nanoparticles or biopolymers with lipid membranes depending on the dimensionality of the system of interest, *i.e.* 3D (liposomes, vesicles…) or 2D (supported bilayers, deposited monolayers…). The information that can be extracted in the different configurations is highly complementary and allows to get a structural and quantitative description of the interaction. While 3D experiments, such as isothermal titration calorimetry (ITC) or dynamic light scattering (DLS) provide the thermodynamic parameters of the interaction and stoichiometry of the aggregation process respectively, the visualization of the interaction of the objects of interest with liposomes or vesicles is still problematic due to the fragility of the lipid constructs, requiring delicate cryo-TEM experiments.

On the contrary, 2D experiments using quartz crystal microbalance with dissipation monitoring (QCM-D) allows a fine tuning of the quantity of nanoparticles deposited on supported lipid bilayers in various environment. This technique enables real-time measurement of adsorption processes in various cases such as ligand-macromolecule binding, electrostatic and non-electrostatic adsorption phenomena, and nanoparticles and thin film deposition, without the need for labeling. [9-13] QCM-D provides information on the adsorbed amount and viscoelastic properties

of the film bound to a sensor crystal, by recording the changes in the crystal resonance frequency, Δf, and in the dissipation energy, ΔD, of the shear oscillation.

More sophisticated experiments like QCM-D combined with D_2O exchange are often used to investigate the water content in a deposited layer by taking profit of the difference in density between heavy and light water .[14, 15]

Another common method to probe thin film architecture is scanning force microscopy (SFM) commonly referred to as atomic force microscopy (AFM). By probing sub-nano Newton force interactions between a sample and a nanometric-sized tip, SFM can measure surface topography at the nanoscopic level, providing local roughness, distribution and structural organization of the adsorbed layer. Soft and weakly bonded biomaterials are better imaged in liquid medium via the pulsed force mode of SFM. In order to determine the film thickness, the contact mode is used to peel off the molecules or particles adsorbed on the surface ('nano-shaving'). Total internal reflection fluorescence microscopy (TIRFM) can also be used to investigate the structural features of thin films since this technique allows for the selective excitation of surface-bound fluorescent molecules such as lipids and proteins, while unbound molecules localized in the bulk of solution are not excited, and thus, do not fluoresce. Due to these advantages, TIRFM has become a preferred method for single molecule detection and tracking[16] as well as for the investigation of biological events involving adsorption of particles on lipid membranes.[17] TIRF was also used to probe the formation of thin films[18] and is a useful tool to probe their homogeneity at a microscopic length scale.

In this context of NP-lipid 2D systems, the case of the interaction of cellulose nanocrystals with lipid bilayers was not considered yet despite its relevance for the design of bioinspired constructs. Cellulose nanocrystals (CNCs) indeed stand out as attractive building blocks since they correspond

to abundant, sustainable materials with excellent mechanical properties and high colloidal stability.[19] In the plant kingdom, the first step in the construction of the primary cell wall is the deposition of cellulose microfibrils on the external leaflet of a lipidic membrane, a process which plays a major role in the mechanical properties of the growing plant.[20, 21] Cellulose nanocrystals (CNCs) can be used as a convenient colloidal model to mimic the naturally occurring cellulose microfibrils. Prepared by sulfuric acid hydrolysis of cellulose fibers from natural sources, these slender nanoparticles having 3 to 20 nm in cross-section and 100 to 3000 nm in length depending on their biological origin, possess negatively charged sulfate ester groups at their surface.[22] In spite of the low degree of substitution (0.2-0.6 e^- nm^{-2})[22, 23], these negative charges are sufficient to grant colloidal stability to the nanoparticles thanks to electrostatic repulsion, making them useful as elementary units for thin film preparation. In fact, cellulose nanocrystals have already been incorporated into biomimetic multilayered thin films deposited on silicon wafers.[24, 25]

However, the literature covering the interaction of CNCs with lipid membranes, that could truly reproduce the living cells in terms of composition and mechanical properties, is still limited. In a previous report we have shown, using light scattering and isothermal titration calorimetry (ITC), that the interaction between CNCs and lipid vesicles was strongly dependent on the charge of the lipid membrane, which could be controlled either by changing the membrane lipid composition or, in the case of zwitterionic lipids, by varying the pH of the suspension.[26]

In this work, we combine QCM-D, SFM and TIRFM data to follow the deposition of CNCs on top of lipid membranes with the aim of identifying key parameters governing the formation of the constructs. We varied the SLBs lipid composition and buffer pH in order to test the effect of these parameters on the adsorption of CNCs on the SLBs. We also used D_2O solvent exchange experiments coupled with QCM-D to get information on the hydration of the deposited layers.

Finally, SFM and TIRFM were used to explore at different length scales the homogeneity of the films and to determine the effect of CNCs concentration in the suspension on the lipidic membrane surface coverage.

Experimental section

Materials

1,2-Dioleoyl-sn-glycero-3-phosphatidylcholine (DOPC) and 1,2-dioleoyl-3 trimethylammonium-propane (DOTAP) and 1-palmitoyl-2-(6-[(7-nitro-2-1,3-benzoxadiazol-4-yl)amino] hexanoyl)-sn-glycero-3-phosphocholine (NBD-PC) (powder, >99% purity) were purchased from Avanti Polar Lipids Inc. (Albaster, AL) and dissolved without further purification in a chloroform/methanol mixture (9/1 v/v) to a total concentration of 10 mg mL^{-1}. The solutions were stored at -20 °C until use. Deionized water from Milli-Q Millipore system with a resistivity of 18.2 Ω cm was used for all experiments. Sucrose, H_2SO_4 and H_2O_2 were purchased from Merck (Merck, France) and used without further purification. Rhodamine B isothiocyanate (RhodB), NaCl, D_20, and Sodium acetate salt ($Na^+CH_3COO^-$,99% pure) were purchased from Sigma Aldrich (France). All chemicals were of analytical grade.

Vesicle preparation

Lipid mixtures (DOPC or DOPC/DOTAP 2:1 molar ratio) dissolved in chloroform were transferred to a round bottom flask and the chloroform was removed by evaporation under vacuum (100 mbar) for five hours. The lipid film was hydrated by vortexing in the appropriate buffer to obtain a lipid concentration of 1 g L^{-1}. Typically, 3 mL of vesicle suspension was obtained. The resulting multilamellar vesicles were sonicated with a tip sonicator (Branson 450, Branson, USA) for 5 minutes in an ice bath until clarity, followed by centrifugation (10 minutes at 20100 RCF,

ambient temperature) to remove the metallic particles detached from the sonicator tip. Before subsequent measurements, the resulting small unilamellar vesicles were diluted to 0.1 g L^{-1} into a solution, which consisted of 200 mM sucrose/10 mM NaCl for pH 6 and 10 mM acetic acid/sodium acetate buffer for pH 3.

CNCs preparation

CNCs suspensions were prepared by acid hydrolysis of cotton linters (Buckeye Cellulose Corporation) according to the method described by Revol et al.[22] The almost pure cellulosic substrate was treated with 65 wt% sulfuric acid for 30 min at 63 °C. The suspensions were washed by repeated centrifugations, dialyzed against distilled water until constant conductivity of the dialysis bath and ultrasonicated for 4 min with a Branson Digital sonifier. After these treatments, the suspensions were filtered through 8 μm followed by 1 μm cellulose nitrate membranes (Sartorius). The resulting aqueous CNCs suspensions had a mass content of 2.0 ± 0.1 wt%. They were then diluted with appropriate amounts of buffer to the desired concentration of 0.0001-1 wt%.

In order to enable their visualization by fluorescence microscopy, the CNCs were labeled with a rhodamine-B fluorophore as described by Nielsen et al.[27] Briefly, following the grafting reaction, the CNCs were centrifuged at 11200 rpm for 30 minutes; the supernatant was then removed and the pellet re-dispersed into a solution of 0.1 M NaOH. This step was repeated twice and followed by dialysis against pure water until neutrality. The purification step was terminated with a rinsing step in an ultrafiltration chamber through a cellulose membrane of 10 kDa. The final product contained 2 wt%. CNCs and was stored at 4 °C until use.

Methods

Dynamic light scattering (DLS) and ζ-potential

DLS and zeta measurements were applied in order to verify the size and charge of the vesicles prior to the SLB deposition. DLS measurements were performed with a Malvern NanoZS instrument operating with a 2 mW HeNe laser at a wavelength of 632.8 nm and a detection angle of 173°. All measurements were done within a temperature-controlled chamber at 20 °C (±0.05 °C). Three measurements of 15 runs each were usually averaged. The intensity size distribution was obtained from the analysis of the correlation function using the cumulants method. The electrophoretic mobility of vesicles and CNCs was measured by using the same Malvern NanoZS apparatus performing at 17° from which the ζ-potential values are determined by applying the Henry equation. The ζ-potential values and the ζ-deviation were averaged over at least three measurements with at least 30 runs per measurement. They were expressed as mean ± SD ($n \geq 3$).

Quartz crystal microbalance with dissipation monitoring (QCM-D)

QCM-D experiments were performed using a Q-Sense E4 instrument (Q-sense, Gothenburg, Sweden) equipped with one to four flow modules. Experiments were conducted under continuous liquid flow of liquid with a rate of 50μL/min, using a multichannel peristaltic pump (ISM 935C Ismatec, Switzerland). The temperature of the solutions was stabilized using a temperature control chamber (Eppendorf, Germany) operated at 24 °C. A clean quartz crystal sensor was placed in the measurement chamber of the flow module; the resonance frequency and the dissipation factor were monitored in air and then in liquid for the fundamental 4.95 MHz as well as for the six odd overtones (n=3-13). Suspensions of small unilamellar vesicles (SUVs) or CNCs were injected into the measurement chamber until a stable baseline was reached (ΔF<1 Hz

and $\Delta D<0.1\ 10^{-6}$ over 10 min). The changes in dissipation and frequency presented here were normalized by the overtone number and reported only for the 7th overtone.

Substrate preparation. Silicon coated AT-cut quartz crystals (QSX 303) were purchased from Biolin Scientific (Stockholm, Sweden). The silicon coated disk shaped had a diameter of 14 mm, a surface roughness<1 nm with a fundamental frequency of 4.95 MHz ± 50 kHz. The sensors were rinsed with a 2 wt% SDS aqueous solution followed by abundant water rinsing and dried under a nitrogen stream. The sensors were then exposed to a UV/ozone lamp for 10 minutes prior to the measurements.

QCM-D data analysis. In the case of homogeneous, quasi-rigid films (for which $\Delta D/-\Delta f << 4\ 10^{-7}$ Hz^{-1}), the frequency shifts are proportional to the mass uptake per unit area (m_{QCM}), which can be deduced from the Sauerbrey relationship:[20]

(1) $m_{QCM} = -C\,\Delta f$

where C is the mass sensitivity of the crystal (17.7 ng cm^{-2} Hz^{-1} at f_1 = 4.95 MHz). In the case of soft films , the adsorbed film was modeled as a homogeneous viscoelastic layer of acoustic thickness d_{QCM}, density ρ, and a complex shear modulus G(f) with a storage modulus G'(f) and loss modulus G''(f) The frequency dependence of the viscoelastic properties was approximated by power laws with exponents α' and α":

(2) $G'(f) = Go'\left(\frac{f}{fo}\right)^{\alpha'}$, $G''(f) = Go''\left(\frac{f}{fo}\right)^{\alpha''}$

where G_0' and G_0'' are the shear storage and loss moduli at a reference frequency, f_0= 35 MHz, d_{QCM} is the film thickness with a density of ρ. ρd_{QCM}, $\rho G_0'$, $\rho G_0'$, α', and α" were adjustable fitting parameters. The semi-infinite bulk solution was taken as water and was assumed to be Newtonian with a viscosity η_l = 0.89 mPa·s at T= 25°C and a density of ρ_l = 1.0 g cm^{-3}. Initially the CNCs film density ρ was fixed to 1.0 g cm^{-3}, without this affecting the generality of the modeling (see

below). Details of the fitting procedure have been described previously [26] and the specified errors represent a confidence level of one standard deviation (68%). The viscoelastic model contains exclusively the product terms $m_{QCM} = \rho d_{QCM}$, $\rho G_0'$, and $\rho G_0''$, and the fitting will therefore provide correct results for these product terms irrespective of the exact choice of ρ. The 5^{th}, 7^{th}, 9^{th}, 11^{th} and 13^{th} overtones were used for the calculation.

Determination of coupled water with D_2O/H_2O solvent exchange: The water content of the film was determined by using a procedure described by Craig et al and by Kittle et al.[27, 28] by changing the water to deuterium oxide and comparing the scaled QCM-D frequency shifts. Water was introduced to the flow cell at a flow rate of 0.1 mL min^{-1} on a bare crystal and on a lipid/CNC film. After reaching a stable base line, D_2O was introduced to the cell for few minutes until a stable baseline was obtained, and the frequency changes was recorded for the bare crystal (Δf_{bare}) and the lipid-CNC film ($\Delta f_{n,film}$). The cells were then rinsed with water until the frequency reached back to the initial value. The reported value is the areal mass of water in ng cm^{-2}.

Scanning force microscopy (SFM)

The SFM measurements were performed with a Dimension ICON instrument from Bruker Company. The surface topography was investigated via a pulsed force (PeakForce) mode, whereas the nano-shaving process was done under contact mode. Both modes were applied *in situ* in liquid medium to avoid the drying of the SLB layer, which led to the CNCs layer disassembly, a situation very different from the conventional deposition on a polymer substrate.

Imaging was performed with an open liquid-cell and a ScanAsyst liquid cantilever-tip having a radius of around 20-30 nm and a spring constant of 0.7 N/m. (manufactory data).

In order to control all probing parameters and better adjust the tip to sample interaction, the SFM data was acquired without ScanAsyst technique. A 50 nm Peakforce amplitude was selected due to the actual low adhesion level and in order to minimize the hydrodynamic forces, which can hinder the measurements. For the same reason, a 1 kHz z-modulation was selected. The PeakForce set-point was kept below the SLB breaking force (i.e. 1 nN for the tip used here). Depending on the density of the CNCs in the film, this setpoint force was adjusted to limit the deformation of the fluid-like SLB below. A force of less than 150 pN was used in the case of a dispersed CNCs layer since the tip pressure is transferred to the SLB via a single cellulose nanocrystal thereby promoting the SLB deformation and in rare cases its disruption. On a contrary, in the case of a dense CNCs layer, a sharp image could be obtained by applying a force of 750 pN. This large force distributes over many CNCs within the layer, thereby promoting less deformation of the fluid-like SLB.

SFM images plotting and their data analysis were achieved with the Gwyddion free software. To extract the thickness of the CNCs layer after nanoshaving, a careful method needed to be followed since the sample surface was rough. A data leveling was first achieved in the well bottom, i.e. the flattest area, by fitting a plane through three points. After plane removing, different line profiles were plotted to control the plane subtraction (see supporting information). Finally, the step height was determined via averaging a maximum of scan lines passing through the well.

Total Internal Reflection Fluorescence microscopy (TIRFM)

Total internal reflection fluorescence microscopy (TIRFM) experiments were carried out with a Leica DMI6000 B microscope. Samples were excited by total internal reflection illumination at 488 and 568 nm and images were captured with an Andor back-illuminated DU-897 EMCCD camera (512X512 pixels) controlled by Leica software (LAS-AF-6000, Leica Microsystems CMS GmbH, Germany). The fluorescence intensity values were evaluated by the Leica LASX software. A region of 50X50 μm^2 (220X220 pixels) was selected and the values were obtained for at least 10 different regions. Error bars indicate the standard deviations for the experimental values ($n \geq 10$).

TIRFM observation and flow cell preparation. The CNCs/SLBs constructs were generated in an observation cell consisting of a microscope glass slide 2X5 cm with parafilm spacers and sealed with a cover slip, creating observation channels with volume of 50 µL and surface of about 1 cm^2 (see figure SI1). The slides and cover slips were cleaned with piranha solution (H_2SO_4 /H_2O_2 70/30 V%), rinsed with ethanol and stored in milli-Q water until used. Prior to the deposition of the layers, the slides were dried under a nitrogen gas flow. The preparation protocol of sample for observation was the following: on a clean cell, a drop of the suspension was deposited on one side of the channel and pulled in due to capillary forces to the other side of the channel. Excess liquid was wicked off using a filter paper placed on the other side of the channel. The flow in the channel was laminar so that exchange of material could be easily performed. During the filling process, care was taken to avoid the formation of bubbles during the flowing.

Formation of the CNC/SLB construct. The deposition of the vesicles was achieved in the following way: first, the channel was rinsed four times with a buffer composed of 200 mM Sucrose and 10 mM NaCl (pH~6). Then a vesicle suspension (DOPC/DOTAP 70/30 %/% mol., 1 gr L^{-1})

was deposited in the cell and incubated for 15 minutes at room temperature. The cell was then rinsed again with 4 volumes of suspension buffer. The SLBs was excited at 488 nm, close to the excitation spectrum maxima of the DOPC-NBD (461 nm). In the second step, a drop of 50 µL of CNCs at the desired concentration ($0\text{-}1\cdot10^{-1}$ wt%) was loaded into the flow cell and incubated for 15 minutes at room temperature and rinsed with four volumes of a 200 mM sucrose solution. We have chosen not to measure higher concentration of CNCs in order to ensure that the system is in the semi-dilute regime and to avoid influence of particle-particle interaction or a change in rheological properties, on the deposition process.

The deposition of the CNCs on top of the lipid bilayer was visualized by fluorescence, at an excitation wavelength of 561 nm, which is close to maximum in the excitation spectrum of Rhod-B (556 nm). A scheme comparing the general configuration of the measurement in each method is described in figure SI1.

Results

QCM-D monitoring of film deposition

QCM-D measurements were used to monitor the formation of the SLBs on the surface of a silicon coated quartz crystal and the subsequent adsorption of CNCs onto the lipidic membrane. SLBs were prepared by fusion onto the quartz crystal of small unilamellar vesicles (SUVs) prepared from three different lipid compositions. The chemical structure of the lipids is shown in Figure SI2. The vesicles were characterized for their size and charge using DLS and ζ-potential measurements. The vesicles charge varied according to the pH of the medium and the lipid composition used. DOTAP containing vesicles showed ζ-potential value of +47.3 mV as expected from the positively charged lipid. For DOPC vesicles, the ζ-potential values at pH 6 and 3 were -

2.1 and +9.5, respectively, the tunable charge of DOPC with pH being associated with its zwitterionic nature.[29] DLS measurements were performed to estimate the average hydrodynamic diameter of the vesicles used to create the SLBs. The z-averaged hydrodynamic diameters extracted from the cumulants fit to the auto-correlation function varied between 60-110 nm for all lipid compositions used with a PDI of 0.20-0.25.

Figure 1 depicts the QCM-D signals resulting from the mass accumulation on the quartz crystal sensor following the deposition process. After reaching a stable baseline, a suspension of SUVs was injected into the measurement chamber (arrow 1), which was followed by a rinsing step with pure water to ensure complete SLBs formation while removing lipids in excess (arrow 2). The water was replaced by the appropriate buffer, either at pH 3 or 6 (arrow 3). When a constant value of frequency and dissipation was achieved, a 0.1 wt%. CNCs suspension was injected into the measurement chamber (arrow 4) followed by rinsing in order to eliminate the excess of non-adsorbed CNCs (arrow 5).

After SUV injection, a decrease in resonance frequency and a small change in dissipation were observed for all the SUV compositions or pH probed. Frequency changes of -24.7, -25.1 and -23.9 Hz were observed for DOPC at pH 3, DOPC at pH 6 and DOPC/DOTAP at pH 6, respectively. These values are in a good agreement with what was expected for the formation of a homogeneous bilayer on top of the quartz crystal sensor.[30, 31] The values of dissipation change were 0.8, 0.3, and $0.1 \cdot 10^{-6}$ for DOPC at pH 6, DOPC/DOTAP at pH 6, and DOPC at pH 3, respectively. These low dissipation values indicate the formation of a compact dense layer at the surface of the crystal, which allowed us to extract the areal mass density from the frequency shifts using the Sauerbrey relationship (equation 1). Values in the range 420-450 ng/cm^2 were calculated for the three SLB layers investigated. Assuming a highly hydrated film with a density close to that of water (1 g/cm^3),

the derived thickness was thus 4.2-4.5 nm, which matches what is expected for a pure phospholipid bilayer. Note that the frequency and dissipation were not significantly influenced by the lipid composition or the pH conditions, in fair agreement with previous observations from DOPC and DOPC/DOTAP membranes.[30] These results show the effective deposition of homogeneous SLBs and indicate that changing the membrane composition or the pH had little or no influence on the SLB formation.

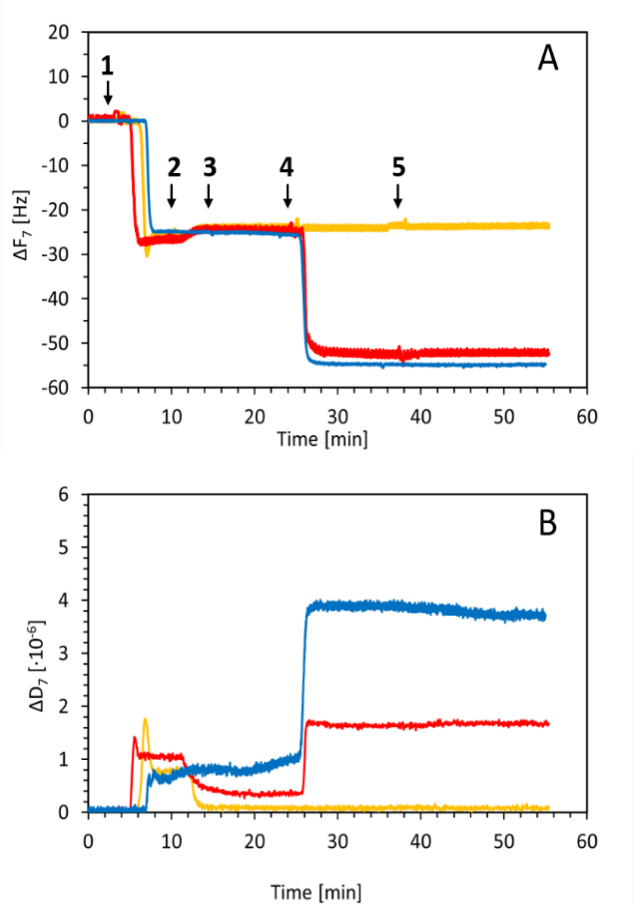

Figure 1. QCM-D profiles showing the changes as a function of time in frequency for the 7th overtone, ΔF_7, (A) and the corresponding dissipation values for the 7th overtone, ΔD_7 (B) following the injection of lipids and CNCs (0.1 wt%) into the measurement chamber for different lipid compositions and pH: DOPC at pH=6 (yellow), DOPC/DOTAP at pH 6 (red) DOPC at pH 3 (Blue). The arrows correspond to the injections of the following solutions or suspensions: 1-vesicles, 2-water, 3-buffer, 4-CNCs and 5-water.

In the subsequent step, the adsorption of CNCs onto the SLBs of various compositions and surface charges was evaluated by QCM-D, following the injection of 0.1 wt% CNC suspensions. A notable decrease in frequency of -27.6 and -29.8 Hz was measured for DOPC/DOTAP at pH 6 and DOPC at pH 3 respectively (red and blue curves in Figure1), showing the successful deposition

of the nanoparticles on top of the SLBs in these systems. Oppositely, no detectable change in frequency could be observed when the SLB was composed of DOPC at pH 6, reflecting that no CNCs adsorption took place in this case. These data qualitatively show that positively charged SLBs are required to make the adsorption of negatively charged CNCs possible. This result is in agreement with our previous observations of a 3D aqueous systems comprising liposomes and CNCs where the charge of the lipid membrane played the main role in the interaction with nanocrystals.[26]

The ΔD values measured as a result of CNCs film deposition were $1.4 \cdot 10^{-6}$ and $2.9 \cdot 10^{-6}$ for the DOPC/DOTAP and DOPC membranes, respectively. The lower dissipation value in the DOPC/DOTAP case may be related to the surface charge of the membrane. The electrostatic attraction in the case of higher lipid charge led to a more rigid layer, while for DOPC at pH 3 - which leads to a zwitterionic membrane- the effect of the surface charge was decreasing rapidly with the distance from the polar head, resulting in weaker attractive forces between the membrane and the CNCs and a more loosely bound layer indicated by the higher dissipation. Nonetheless, both films showed relatively low dissipation values, implying that in both cases the CNC layer was indeed coupled to the SLB surface. The presence of an adsorbed CNC layer is further evidenced by the fact that the frequency and dissipation curves remained stable following the subsequent rinsing step.

Given the low dissipation values, the SLB layer thickness could be estimated directly from the Sauerbrey relationship (equation 1), however, in order to estimate the CNC layer thickness, a viscoelastic model should be applied. Table 1 provides a summary of the results obtained from the QCM-D experiments. The values shown in the table are derived from average value frequency and dissipation changes for the 7^{th} overtone, ΔF_7 and ΔD_7, measured over a stable region (minutes 17-

22 for SLB and 44-52 for CNCs) and considering initial value of zero for both frequency and dissipation.

Table 1. Quantitative analysis of the QCMD curves for SLBs and CNCs deposited on SLBs films. [a]Estimation based on the ζ- potential values of the SUVs from which the bilayer was formed. [b]Values obtained using Sauerbrey relationship (see materials and methods). [c]Values extracted from small load approximation analysis using the QTM software (see text for details).

DOPC /DOTAP Molar ratio	pH	ζ-potential [mV][a]	Δf_{SLB} [Hz]	ΔD_{SLB} [$\cdot 10^{-6}$]	Δm_{SLB}[b] [ng cm^{-2}]	Δf_{CNC} [Hz]	ΔD_{CNC} [$\cdot 10^{-6}$]	Δm_{CNC} [ng cm^{-2}]	d_{CNC}[c] [nm]
2:1	6	+47.3	-24.7	0.3	445.0	-27.6	1.4	565	5.7 (-0.3/+9.7)
1:0	6	-2.1	-25.1	0.8	436.6	+0.2	0.1	N/A	N/A
1:0	3	+9.5	-23.9	0.1	423.1	-29.8	2.9	668	6.7 (-0.2/+1.1)

The values for the CNC layer thickness were calculated using the QTM software considering the CNC layer as a homogeneous viscoelastic layer. The model takes as an input the frequency and dissipation changes measured for each overtone and extracts the thickness for a given density with respect to a reference state, usually taken as pure water (which is justified by the very hydrated state of the layer). A quantitative analysis based on this model yielded adsorbed amounts of 565 and 668 ng for the DOPC/DOTAP SLB at pH 6 and the DOPC SLB at pH 3, respectively.

In the following experiments we focused on the adsorption of CNCs on the DOPC/DOTAP membrane since it was found to be more robust and enabled working at nearly neutral pH while avoiding possible contributions from the addition of different salts usually needed for buffer solutions.

Estimation of CNCs water content using D_20/H_20 solvent exchange

In order to better estimate the water content of the CNC film adsorbed on the SLB, we used a D_2O/H_2O solvent exchange procedure.[14, 15] In this method, the difference in the normalized frequency between the bare crystal and the film, following the exchange of water with D_2O, is used for the calculation of coupled water according to equations (3) and (4), as follows:

(3) $$(\Delta f_n)_{water} = \frac{(\Delta f_n)_{film} - (\Delta f_n)_{bare}}{\left(\frac{\rho_{D_2O}}{\rho_{H_2O}}\right) - 1}$$

Where ρ_{D_2O} and ρ_{H_2O} are the densities of D_2O and H_2O respectively, (1.106 and 0.998 g cm^{-3} at 25°C), $\Delta f_{n,bare}$ and $\Delta f_{n,film}$ are the recorded frequency changes due to the exchange of D_2O with water for the bare crystal and the film respectively. For the case where the layer is composed of the film and exchangeable water, then $\Delta f_{n,film}$ will contain the contribution from the crystal and the film plus exchangeable water. $\Delta f_{n,water}$ can then be calculated from the difference between $\Delta f_{n,bare}$ and $\Delta f_{n,film}$ according to equation 3 and the surface concentration, Γ_{water} ,is calculated from equation

(4) $$\Gamma_{water} = -C \cdot (\Delta f_n)_{water}$$

Where C is a constant, equal to 17.7 ng cm^{-2} Hz^{-1}.

Figure 2 shows the normalized frequency for the 7th overtone, obtained from the exchange of D_2O and water for the bare crystal (dashed black line) and the film (solid red line). The experiment was done for DOPC/DOTAP SLB composition, where CNC adsorption is possible in pure water.

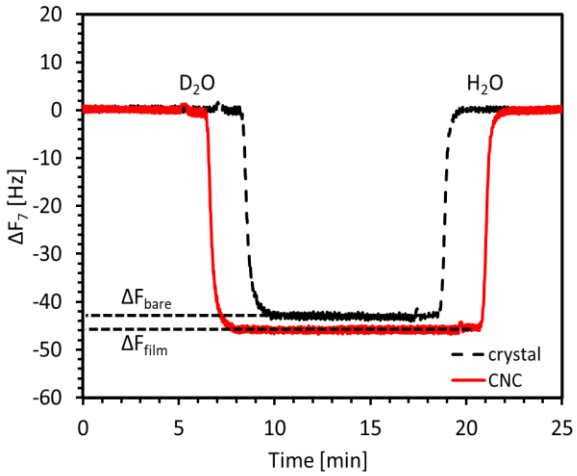

Figure 2. Normalized frequencies (n=7) following D_2O/H_2O exchange procedure for the bare crystal (dashed black line), and for the film (solid red line).

The normalized frequencies at the 7th overtone were recorded and found to be -45.6±1.1 Hz and -43.3±0.6 Hz (mean±SD, n≥3) for the film and the bare crystal, respectively. Γ_{water} was then calculated for the film according to equations 3 and 4 and was found to be 380±90 ng cm^{-2}. Since the film is hydrated, its acoustic areal mass density (hydrated mass) will thus be composed of the areal mass densities of the CNCs and the hydrodynamically coupled water molecules and counterions. In order to estimate the amount of bound water, we have performed a solvent exchange experiment. The frequency differences obtained (Figure 2) were used for the calculation of the areal water mass using equations (3) and (4) yielding water mass uptake of 380 ng cm^{-2}. The hydrated mass obtained for the same type of film was 565 ng cm^{-2} resulting in dry mass of 185 ng cm^{-2}. The amount of water in the film may be directly derived from the hydrated and water masses and was found to be 67±15%.

Microscopic visualization of the constructs using TIRFM

In order to investigate the structural properties of the CNC/SLB constructs at tens of micrometers length scale, TIRF microscopy was used to directly image the formation of the lipid bilayer and the deposition of the CNCs on top of it. Especially, the effect of the concentration of the CNC suspension on the formation and homogeneity of CNCs/SLBs films was investigated. CNCs samples were prepared from dilution of a 1% CNCs aqueous suspension at pH 6 and the resulting sample concentration varied from 0 to 0.1 wt%. We did not use 1 wt% sample in order to avoid viscosity variations which can influence the flow in the cell.

The experiments were performed in the flow chamber described in the experimental section, which is commonly used for biophysical studies.[32] In order to visualize the SLB and CNCs independently, two different fluorescent probes were used: lipidic membranes were labeled using NBD-PC and CNCs using rhodamine B (see experimental section for details). Figure 3 depicts the impact of CNCs concentration using 45×45 μm^2 top view images of the films in the case of SLB-only visualization (top row), CNCs-only visualization (middle row) and co-visualization (bottom row).

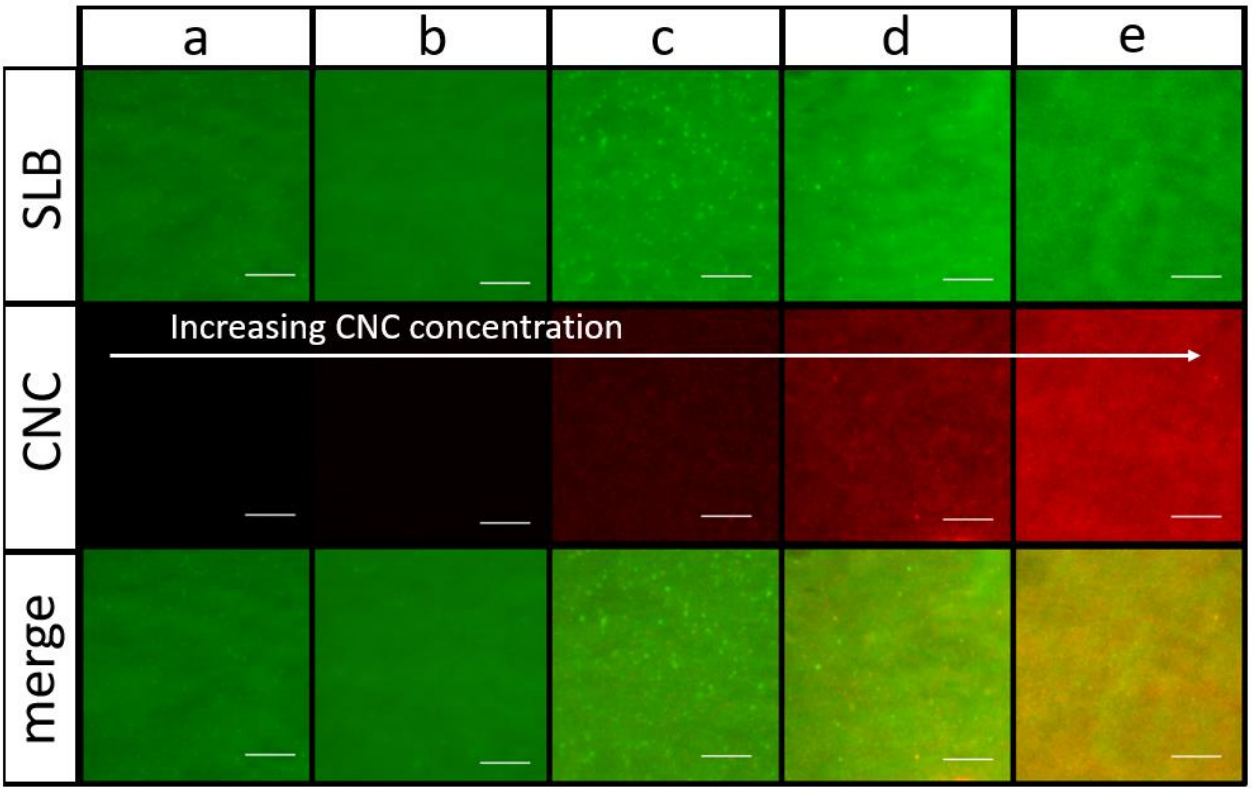

Figure 3. TIRF images of SLB-CNC thin films recorded with two excitation modes simultaneously on the same region of interest with increasing CNC concentrations: 0 (a), 1.10^{-4} (b), 1.10^{-3} (c), 0.01 (d) and 0.1 wt% (e). Top: DOPC-NBD SLB signal (excitation at 488 nm), middle: CNC-RhodB signal (excitation at 568 nm) bottom: overlay of the two channels. The images were recorded under the same acquisition conditions for all samples. The scale bar is 10 µm.

As shown in the top row in Figure 3, the images confirm the presence of a homogeneous defect-free SLBs at a ten microns length scale in the observation cell irrespective of the CNC concentration used. In Figures 3c and 3d, bright spots, most likely resulting from clusterization of NBD-PC fluorophores, can be observed. However, it appears that the clusters had no apparent influence on the bilayer homogeneity nor on the fluorescence signal, as will be shown below. Since the same SLB deposition protocol and membrane composition were used for all samples, the fact

that the fluorescence intensity remained roughly constant, using the same acquisition parameters, merely demonstrates the reproducibility of the SLB deposition protocol, enabling to examine directly the effect of CNCs concentration on its deposition. In addition, the deposition of CNCs did not cause SLB removal or disruption as demonstrated by the fluorescence homogeneity on the merged image (bottom row in Figure 3).

In order to quantify the variation in fluorescence intensity and the homogeneity of the lipid bilayer, we have performed a statistical analysis of the fluorescence intensity on a series of TIRF images. It is important to mention here that the quantification of the fluorescence signal should be carried out and interpreted carefully due to the number and experimental sensitivity of the parameters that can influence the signal. To ensure the proportionality of the measured signal to the amount of fluorophore in the sample, we have kept the acquisition parameters (*i.e.* laser intensity, exposure time and camera gain) constant while varying only the CNCs concentration. Figure 4 shows the average fluorescence values obtained from a statistical analysis of the images using the green (SLBs visualization) and red (CNCs visualization) channels for each CNCs concentration for a given region of interest. Typically, 10 regions were averaged and the errors were expressed as the standard deviation from this population (n±SD).

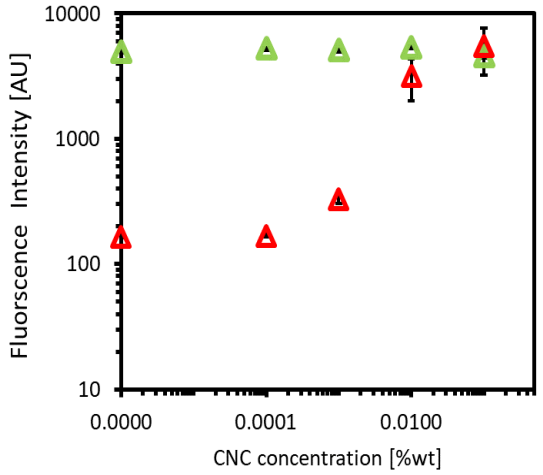

Figure 4. Average fluorescence intensity as a function of CNC concentration for the SLB (green triangles) and CNC layer (red triangles). Values correspond to mean ± SD (n=10).

While the average fluorescence intensity of the SLBs remained roughly constant within measurement error at 5070±320 AU, the fluorescence intensity of the CNCs layer increased with the increase in CNCs concentration tending to a plateau around 0.01 wt%. For CNCs concentrations of 0 and $1 \cdot 10^{-4}$ wt%, no fluorescence was observed above the noise level of 164±2 AU, determined from the intensity value at zero CNCs concentration. An intermediate value of 327±24 AU was observed at $1 \cdot 10^{-3}$ wt%, and at 0.01 and 0.1 wt%. the fluorescence intensity reached values of 3000±1180 and 5290±2250 AU, respectively. Data shown in Figures 3 and 4 confirm the deposition of a complete SLBs followed by adsorption of CNCs. The homogeneity of the independent layers and the resulting film in the micron scale was independent of CNCs concentration.

Constructs probed at the nanoscale by scanning force microscopy (SFM)

In order to locally probe the CNCs layer formation at the nanometric scale, we have performed SFM measurements in hydrated conditions. Samples for SFM were prepared under the same conditions as for a typical QCM-D experiment. A lipid bilayer was deposited on a quartz crystal in an open module which enables the removal of the crystal from the QCM platform and directly transferring it to the SFM instrument, while avoiding the drying of the sample. The samples were them characterized by SFM in liquid medium in order to investigate at the nanoscale the coverage, density and structure of the CNC layer deposited on the SLB in its hydrated state. A typical image of the surface topography is shown in Figure 5A. It needs to be noted that an image of very good quality, comparable to what is usually reported for dried films, could be obtained. It reveals that the surface is almost fully covered by CNCs. Identical dense CNCs layers were observed when probing different areas of one sample or by investigating different samples, which confirms the homogeneity and robustness of SLB formation and CNC adsorption. A few nanocrystals still remained on the top of the dense layer even if several rinsing steps right after the deposition were applied. Being further away from the SLB surface such that the electrostatic interactions are lower, these CNCs are not strongly bounded causing some image blurring. A z-averaged profile of 128 scan lines taken around the white line in Figure 5A is presented in Figure 5B. The roughness of the continuous film at the nanoscale level can easily be seen. In addition, isolated CNCs of 8 nm characteristic height can be detected. Data therefore show that the adsorption of CNCs onto the SLBs occurred as a dense monolayer on top of which scarcely distributed CNCs were detected. This result is in full agreement with QCM-D data showing that the thickness of the adsorbed CNCs layer is 6-7 nm.

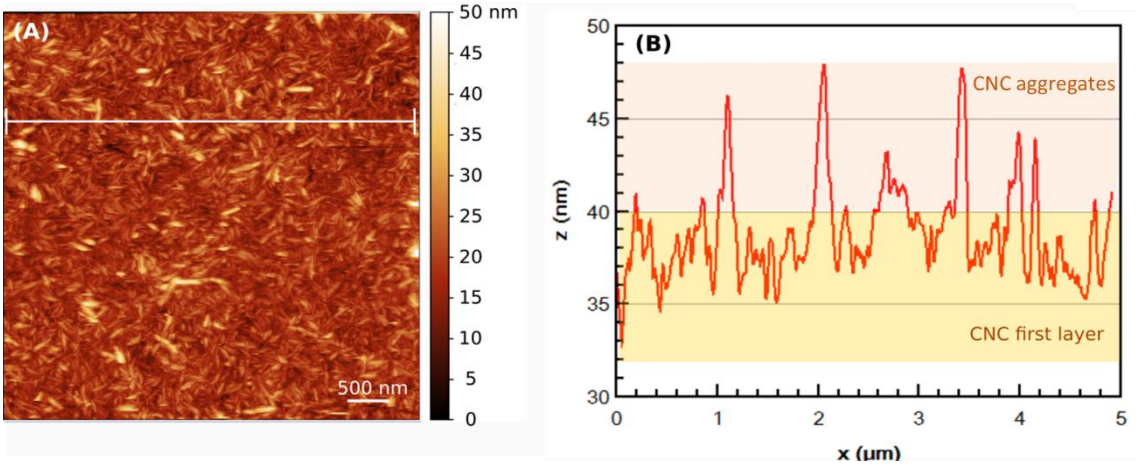

Figure 5. (A) Topography of SLBs/CNCs layer made from DOPC/DOTAP 70/30 %mol. at pH 6, on quartz substrate obtained by SFM in Peakforce mode in Milli-Q water. The PeakForce setpoint was 100 pN. Image is plotted after removing polynomial background, aligning rows and correcting horizontal scars. (B) Z-profile averaged over the 128 lines marked by the white line and its borders in Figure 5a. Coloured rectangles with 8 nm in height were added as an indication for the CNCs height. Few isolated CNCs lying on top of the construct are also clearly visible.

A nanoshaving of the CNC-covered SLB film was performed in order to precisely determine the construct thickness. This procedure was performed in contact mode. In order to determine the working conditions, different tip loadings, *i.e.* friction forces, were first tested. As an optimum parameter, the lowest force of 0.5 V cantilever-tip deflection was chosen to remove the layer without needing to use of a very blunt tip (see supporting information). A 1x1 μm^2 surface area was thus scanned in both directions (0 and 90 degrees) with a large number of lines (i.e. 1024), guarantying the shaving quality. The result of this process is presented in Figure 6. This 3x3 μm^2 topography image was recorded using the non-invasive Peakforce mode and in the same liquid medium. Note that the surface that was not subjected to nanoshaving remained intact. However, the use of a blunt tip resulted in a doubling of the lateral size of the CNCs (from 20 to 40 nm). It

can clearly be seen that the nanoshaving process resulted in the formation of a squarish well in the area where the hard contact mode was applied. As expected, the roughness inside the well (dark area in Figure 6) has the same value as that of the quartz substrate, proving that both the CNCs layer and the SLBs have been removed. A z-averaged profile over 64 scanning lines taken along the white line in Figure 6A is presented in Figure 6B. This plot shows the roughness of the continuous film and the presence on top of it of some isolated particles in the range of 8 nm, comparable to the height of one CNCs. The SLBs/CNCs construct thickness appears to be 13 nm ± 3 nm. These data are consistent with the deposited film being composed of a 5 nm thick SLB covered by a dense monolayer of CNCs, with some isolated crystals on top. These values are in good agreement with the values obtained from QCM-D data when taking the total resonance frequency shift (i.e SLBs + CNCs layers). Similar nanoshaving measurements were performed using a much higher 5V cantilever-tip deflection and the same step height was obtained (data not shown), confirming the validity of the results.

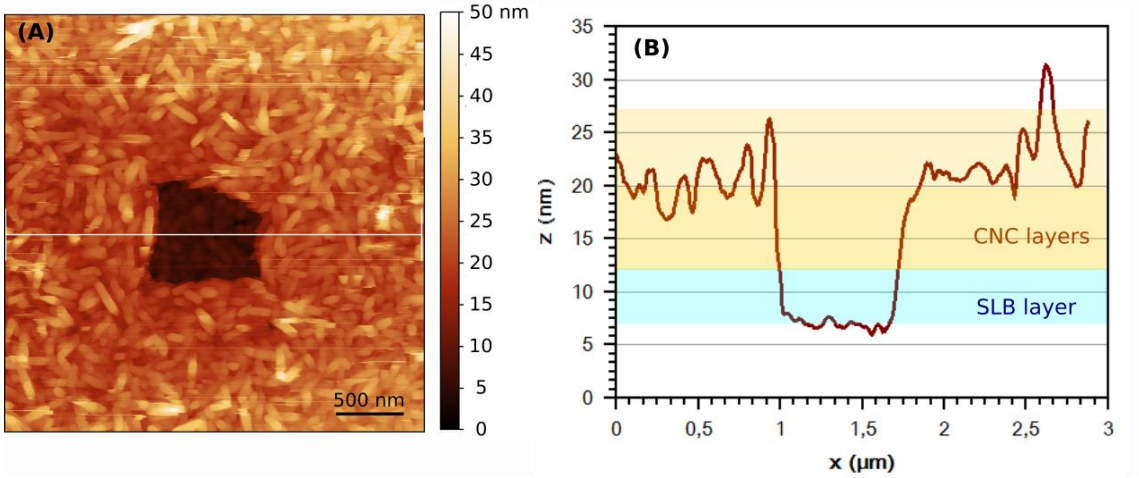

Figure 6. (A) Topography image of a SLB/CNC film on a quartz substrate made from DOPC/DOTAP 70/30 %mol. at pH 6 obtained by SFM in Peakforce mode in Milli-Q water. The Peakforce setpoint was 100 pN. Image was plotted after removing polynomial background, aligning rows and correcting horizontal scars. (B) Z-averaged profile over the 128 lines marked by the white line and its borders in Figure 6a. Coloured rectangles were added as an indication for the CNC height. Few isolated CNC lying on top of the construct are also clearly visible.

The results obtained from the SFM experiments were compared to the QCM-D observations and the derived layer thickness calculation thereafter. Several aspects emerge from this comparison - the estimation of layer thickness, water content and homogeneity will be discussed in the following sections.

Discussion

Several studies have shown that cellulose based films are swollen in aqueous medium, the amount of water being dependent on the nature of the cellulose (native, regenerated…) and mode of deposition (spin coating, dipping…). In an early study, Aulin et al.[33] estimated the water content of cellulose films prepared in different conditions and measured 26% for spin coated CNC films

by evaluating a normalized adsorbed mass measured by QCM-D and thicknesses by ellipsometry after exposure to a buffer solution. Later on, Niinivarra et al. found values of water by mass ranging from 22% for the thicker films to 46% for the thinner one from QCM-D and ellipsometry experiments on CNCs films obtained by spin coating and exposed to a relative humidity of 97%.[34] It is worth mentioning that since the case of relative humidity is different from the case of swelling in liquid water, different behavior is expected. Reid et al. found that swollen CNC films also prepared by spin coating contained 35% wt. water. [35] It has to be noted that all these results are obtained on films that have been prepared by spin coating followed by a drying step that gives a cohesion to the film.

Values of 74 %wt. water by mass have been measured by Kittle et al. [15] for nanocrystalline cellulose films with various thicknesses as measured by ellipsometry, deposited by electrospinning at different concentration, dried and then rehydrated. They have estimated the water content using H_2O/D_2O solvent replacement on the CNCs films deposited on a QCM-D crystal. These results are significantly different from the one evaluated from combined QCM-D and ellipsometry measurements, that evaluate lower amounts of water.

It has to be noticed that in addition, neutron reflectometry measurements on phospholipid bilayers revealed a bound water layer between the substrate and the hydrophilic head, up to 7% of water by volume in the hydrophobic tails region and up to 35% in the head group region.[36, 37] This should account for additional adsorbed water molecules, which can also contribute to the total mass fraction of water in our film, but to a limited extent.

In our case, by knowing the adsorbed masses we may calculate a corrected film density by using equation 5:

$$\rho_{film} = \frac{m_{QCMD}}{\frac{m_{dry}}{\rho_{CNC}} + \frac{m_{water}}{\rho_{water}}} \quad (5)$$

Where ρ_{film} is the film density, m_{QCMD} is the hydrated mass, m_{dry} and m_{water} are the dry and water mass respectively and ρ_{CNC} and ρ_{water} are the densities of cellulose and water respectively. The film density obtained from this calculation was 1.14 g cm^{-3}. By using the calculated density value as the input value in the viscoelastic model, assuming the same water uptake for both films, we obtain thicknesses of 5.7 and 6.7 for the DOPC/DOTAP and DOPC films, respectively.

The best fit of QTM modeling of QCM-D data for the CNCs layer thickness from the model in the case of DOPC/DOTAP system (5.7 nm) is slightly lower compared to the known dimensions of CNCs from cotton prepared under the same conditions (7.5±1 nm) and compared to the thickness measured by us using SFM (8.0±2 nm). Indeed, the value given for the thickness represents the minimum solution, yet thickness with 1 standard deviation (0.683) is in the range of 5.4-14.2 nm and 6.5-7.5 nm for the DOPC/DOTAP and DOPC system, respectively. The X^2 landscape calculated for both systems is shown in the supplementary information (Figure SI3). For the DOPC case the X^2 landscape comprises a skewed bell shape distribution, where for the DOPC/DOTAP system, a single sharp minimum appears around d=5.6 nm followed by a secondary smeared minimum around d=8 nm. The values of thicknesses consistently fall in the range of the estimated layer thickness from SFM , 13±3 nm,for the total film thickness SLB+CNC.

It can be therefore estimated that the positively charged SLBs surfaces are covered by a monolayer of CNCs, on average, with some loosely bound isolated crystal on top of it. This situation is reminiscent of the case of the adsorption of double layers of CNCs onto positively charged poly(allylamine hydrochloride) (PAH) polymer layers, which was ascribed to charge complexation and counterions release effects.[38] In the case of CNCs adsorbed onto PAH, it was further shown that the second layer was twice less dense that the first one.

Theoretically, if all the surface is covered with one layer of cellulosic material, the areal mass is equal to the mass of a cylinder with thickness of 7 nm multiplied by the cellulose density, 1.5 g cm^{-3}. This calculation gives 1050 ng cm^{-2}, representing the maximum dry mass in case of perfect packing. The adsorbed dry masses in our case were 185 ng cm^{-2} for the DOPC/DOTAP, which infers a lower surface coverage compared to the ideal case. The SFM images support this observation, showing that the CNC are randomly distributed, leading to a porous network of entangled rods.

Taking the average film thickness from SFM measurements, the water content from D_2O/H_2O exchange experiment and the maximum estimation from QTM model for DOPC/DOTAP system, we converge to a CNC hydrated layer comprised of about 70-80 %wt. water with a total thickness of 6- 8 nm.

In summary, our results showed that the water content of our deposited layers account for more than 2/3 of the total mass, in agreement with Kittle et al.[15] results but in fair contrast with other estimation from combined ellipsometric and QCM-D measurements, which lead to values closer to 1/4 water content. However, evaluation of random packing of rods in the case of sedimentation of colloids or compaction of anisotropic powders leads to volume fraction at maximum compaction that strongly decrease with increasing aspect ratio, especially for the longer ones.[39]If compacity around 0.6 can be expected in the case of sphere, the maximum volumic fraction for anisotropic particles is 0.3 for an aspect ratio of around 10, 0.2 for 40 and 0.1 for 80. Even if an average aspect ratio of CNC is rather difficult to precisely evaluate, as they are constituted of polydisperse particles with dimension around 7*21*150 nm[40], a rough estimation based on a circumscribed cylinder gives an aspect ratio around 10, leading to an expected compacity of 0.3 that is 70% of water, in fair agreement with our results. Consequent variations

around the estimated aspect ratio of 10 will not change that much the maximum compacity. Whether compacity values as high as 0.75 (around 25% of water) obtained for different CNC's systems as previously mentioned are due to preparation (especially compaction upon drying) and/or substrate differences, or systematic methodologic deviation is clearly beyond the scope of this paper.

Conclusion

We have demonstrated and characterized here the controlled deposition of CNCs on top of a lipid bilayer. The adsorption of the CNC particles and the layer viscoelastic properties were found to be dependent on the charge of the lipid membrane. As expected, a positive charge of the membrane (DOPC/DOTAP at pH=6 and DOPC at pH=3) resulted in a quantitative deposition of a CNCs layer, while for the negative charged membrane (DOPC at pH=6), CNC adsorption was not observed as evidenced by QCM-D experiments. However, the loosely charged system of zwitterionic DOPC at pH=3 exhibited a more dissipative behavior and conditions far from biological systems.

Considering the low dissipation values obtained by QCM-D for the DOPC/DOTAP at pH=6 system, the reproducibility and the crystal dimensions, it is likely that the cellulose adsorbs as a cohesive but loose monolayer on top of the SLBs in the case of positively charged membranes. SFM and TIRF images confirmed the formation of SLBs and showed homogenous CNCs coverage at the micrometer scale, while QCM-D measurements were used to extract the value of the adsorbed CNCs hydrated mass at saturation of about 600±70 ng and an approximated height of 6-8 nm. This height was confirmed via SFM nanoshaving. QCM-D experiments using solvent exchange with D_2O demonstrate the formation of a continuous monolayer of CNCs on top a lipid membrane with a compacity around 0.3, and shed light on the key factors governing the

interactions of these two bio-based building blocks. This study thus demonstrates the feasibility of the controlled deposition of cellulose on top of lipid bilayers that mimic the first step of the cellulose deposition on the plasma membrane inside the plant cell wall, analogous to the many attempts that has been made for animal cells. Whether this model is relevant for the design of biomimetic constructs reproducing plant cell wall will be the object of further studies. It nevertheless paves the way for the design of original bidimensional materials including lipids and cellulose nanocrystals.

ASSOCIATED CONTENT

Supporting information: A scheme of the experimental configuration; chemical structures of the lipid vesicles used for QCM-D experiments; χ^2 landscape for the small load approximation model, SFM supplementary images. (PDF file)

AUTHOR INFORMATION

Corresponding Author

*To whom correspondence should be addressed:

laurent.heux@cermav.cnrs.fr

bernheim@bgu.ac.il

Author Contributions

The manuscript was written through contributions of all authors. All authors have given approval to the final version of the manuscript.

ACKNOWLEDGMENT

The authors would like to thank the nano-bio platform at ICMG, DCM, University of Grenoble Alpes (ICMG FR 2607) for the use of QCM-D and SFM as well as the Glyco@Alps program (Investissements d'Avenir grant No. ANR-15-IDEX-02). YN would like to thank the Negev scholarship for funding and the Ilze katz institute, Ben Gurion University for the use of TIRF platform.

ABBREVIATIONS

CNCs, Cellulose nanocrystals; QCM-D, Quartz crystal microbalance with dissipation monitoring; SFM, scanning force microscopy; TIRFM, total internal reflection fluorescence microscopy; SLB, supported lipid bilayers; DOPC, 1,2-Dioleoyl-sn-glycero-3-phosphatidylcholine; DOTAP. 1,2-dioleoyl-3 trimethylammonium-propane; NBD-PC, 1-palmitoyl-2-(6-[(7-nitro-2-1,3-benzoxadiazol-4-yl)amino] hexanoyl)-sn-glycero-3-phosphocholine; RhodB, Rhodamine B isothiocyanate.

REFERENCES

(1) Contini, C.; Schneemilch, M.; Gaisford, S.; Quirke, N., Nanoparticle–membrane interactions. *J. Exp. Nanosci.* **2018,** *13* (1), 62-81.

(2) Bunker, A.; Magarkar, A.; Viitala, T., Rational design of liposomal drug delivery systems, a review: combined experimental and computational studies of lipid membranes, liposomes and their PEGylation. *Biochim. Biophys. Acta, Biomembr.* **2016,** *1858* (10), 2334-2352.

(3) Boudou, T.; Crouzier, T.; Ren, K.; Blin, G.; Picart, C., Multiple functionalities of polyelectrolyte multilayer films: new biomedical applications. *Adv. Mater.* **2010,** *22* (4), 441-467.

(4) Lorent, J. H.; Levental, I., Structural determinants of protein partitioning into ordered membrane domains and lipid rafts. *Chem. Phys. Lipids* **2015,** *192*, 23-32.

(5) Binder, W. H.; Sachsenhofer, R.; Farnik, D.; Blaas, D., Guiding the location of nanoparticles into vesicular structures: a morphological study. *Phys. Chem. Chem. Phys.* **2007,** *9* (48), 6435-6441.

(6) Wang, B.; Zhang, L.; Bae, S. C.; Granick, S., Nanoparticle-induced surface reconstruction of phospholipid membranes. *Proc. Natl. Acad. Sci.* **2008,** *105* (47), 18171-18175.

(7) Laurencin, M.; Georgelin, T.; Malezieux, B.; Siaugue, J.-M.; Ménager, C., Interactions between giant unilamellar vesicles and charged core− shell magnetic nanoparticles. *Langmuir* **2010,** *26* (20), 16025-16030.

(8) Roiter, Y.; Ornatska, M.; Rammohan, A. R.; Balakrishnan, J.; Heine, D. R.; Minko, S., Interaction of nanoparticles with lipid membrane. *Nano Lett.* **2008,** *8* (3), 941-944.

(9) Kontturi, E.; Tammelin, T.; Österberg, M., Cellulose—model films and the fundamental approach. *Chem. Soc. Rev.* **2006,** *35* (12), 1287-1304.

(10) Olszewska, A.; Junka, K.; Nordgren, N.; Laine, J.; Rutland, M. W.; Österberg, M., Non-ionic assembly of nanofibrillated cellulose and polyethylene glycol grafted carboxymethyl cellulose and the effect of aqueous lubrication in nanocomposite formation. *Soft Matter* **2013,** *9* (31), 7448-7457.

(11) Villares, A.; Moreau, C.; Capron, I.; Cathala, B., Impact of ionic strength on chitin nanocrystal- xyloglucan multilayer film growth. *Biopolymers* **2014,** *101* (9), 924-930.

(12) Alves, N. M.; Picart, C.; Mano, J. F., Self assembling and crosslinking of polyelectrolyte multilayer films of chitosan and alginate studied by QCM and IR spectroscopy. *Macromol. Biosci.* **2009,** *9* (8), 776-785.

(13) Reviakine, I.; Johannsmann, D.; Richter, R. P., Hearing What You Cannot See and Visualizing What You Hear: Interpreting Quartz Crystal Microbalance Data from Solvated Interfaces. *Anal. Chem.* **2011,** *83* (23), 8838-8848.

(14) Craig, V. S.; Plunkett, M., Determination of coupled solvent mass in quartz crystal microbalance measurements using deuterated solvents. *J. Colloid Interface Sci.* **2003,** *262* (1), 126-129.

(15) Kittle, J. D.; Du, X.; Jiang, F.; Qian, C.; Heinze, T.; Roman, M.; Esker, A. R., Equilibrium water contents of cellulose films determined via solvent exchange and quartz crystal microbalance with dissipation monitoring. *Biomacromolecules* **2011,** *12* (8), 2881-2887.

(16) Jaqaman, K.; Loerke, D.; Mettlen, M.; Kuwata, H.; Grinstein, S.; Schmid, S. L.; Danuser, G., Robust single-particle tracking in live-cell time-lapse sequences. *Nat. Methods* **2008,** *5* (8), 695.

(17) Axelrod, D., Total internal reflection fluorescence microscopy in cell biology. *Traffic* **2001,** *2* (11), 764-774.

(18) Blacklock, J.; Vetter, A.; Lankenau, A.; Oupický, D.; Möhwald, H., Tuning the mechanical properties of bioreducible multilayer films for improved cell adhesion and transfection activity. *Biomaterials* **2010,** *31* (27), 7167-7174.

(19) Habibi, Y.; Lucia, L. A.; Rojas, O. J., Cellulose nanocrystals: chemistry, self-assembly, and applications. *Chem. Rev.* **2010,** *110* (6), 3479-3500.

(20) York, W. S.; Darvill, A. G.; McNeil, M.; Stevenson, T. T.; Albersheim, P., Isolation and characterization of plant cell walls and cell wall components. In *Methods in enzymology*, Elsevier: 1986; Vol. 118, pp 3-40.

(21) McNeil, M.; Darvill, A. G.; Fry, S. C.; Albersheim, P., Structure and function of the primary cell walls of plants. *Annu. Rev. Biochem.* **1984,** *53* (1), 625-663.

(22) Dong, X. M.; Revol, J.-F.; Gray, D. G., Effect of microcrystallite preparation conditions on the formation of colloid crystals of cellulose. *Cellulose* **1998,** *5* (1), 19-32.

(23) Foster, E. J.; Moon, R. J.; Agarwal, U. P.; Bortner, M. J.; Bras, J.; Camarero-Espinosa, S.; Chan, K. J.; Clift, M. J.; Cranston, E. D.; Eichhorn, S. J., Current characterization methods for cellulose nanomaterials. *Chem. Soc. Rev.* **2018,** *47* (8), 2609-2679.

(24) Cerclier, C.; Cousin, F.; Bizot, H.; Moreau, C. l.; Cathala, B., Elaboration of spin-coated cellulose-xyloglucan multilayered thin films. *Langmuir* **2010,** *26* (22), 17248-17255.

(25) Jean, B.; Heux, L.; Dubreuil, F.; Chambat, G.; Cousin, F., Non-electrostatic building of biomimetic cellulose− xyloglucan multilayers. *Langmuir* **2008,** *25* (7), 3920-3923.

(26) Navon, Y.; Radavidson, H.; Putaux, J.-L.; Jean, B.; Heux, L., pH-Sensitive Interactions between Cellulose Nanocrystals and DOPC Liposomes. *Biomacromolecules* **2017,** *18* (9), 2918-2927.

(27) Nielsen, L. J.; Eyley, S.; Thielemans, W.; Aylott, J. W., Dual fluorescent labelling of cellulose nanocrystals for pH sensing. *Chem. Commun.* **2010,** *46* (47), 8929-8931.

(28) Eisele, N. B.; Andersson, F. I.; Frey, S.; Richter, R. P., Viscoelasticity of thin biomolecular films: a case study on nucleoporin phenylalanine-glycine repeats grafted to a histidine-tag capturing QCM-D sensor. *Biomacromolecules* **2012,** *13* (8), 2322-2332.

(29) Makino, K.; Yamada, T.; Kimura, M.; Oka, T.; Ohshima, H.; Kondo, T., Temperature- and ionic strength-induced conformational changes in the lipid head group region of liposomes as suggested by zeta potential data. *Biophys. Chem.,* **1991,** *41* (2), 175-183.

(30) Richter, R.; Mukhopadhyay, A.; Brisson, A., Pathways of lipid vesicle deposition on solid surfaces: a combined QCM-D and AFM study. *Biophys. J.* **2003,** *85* (5), 3035-3047.

(31) Richter, R. P.; Brisson, A. R., Following the formation of supported lipid bilayers on mica: a study combining AFM, QCM-D, and ellipsometry. *Biophys. J.* **2005,** *88* (5), 3422-3433.

(32) Gilboa, B.; Gillo, D.; Farago, O.; Bernheim-Groswasser, A., Bidirectional cooperative motion of myosin-II motors on actin tracks with randomly alternating polarities. *Soft Matter* **2009,** *5* (11), 2223-2231.

(33) Aulin, C.; Ahola, S.; Josefsson, P.; Nishino, T.; Hirose, Y.; Österberg, M.; Wågberg, L., Nanoscale Cellulose Films with Different Crystallinities and Mesostructures-Their Surface Properties and Interaction with Water. *Langmuir* **2009,** *25* (13), 7675-7685.

(34) Niinivaara, E.; Faustini, M.; Tammelin, T.; Kontturi, E., Water vapor uptake of ultrathin films of biologically derived nanocrystals: quantitative assessment with quartz crystal microbalance and spectroscopic ellipsometry. *Langmuir* **2015,** *31* (44), 12170-12176.

(35) Reid, M. S.; Villalobos, M.; Cranston, E. D., Cellulose nanocrystal interactions probed by thin film swelling to predict dispersibility. *Nanoscale* **2016,** *8* (24), 12247-12257.

(36) Montis, C.; Gerelli, Y.; Fragneto, G.; Nylander, T.; Baglioni, P.; Berti, D., Nucleolipid bilayers: A quartz crystal microbalance and neutron reflectometry study. *Colloids Surf., B* **2016,** *137*, 203-213.

(37) Wacklin, H. P., Neutron reflection from supported lipid membranes. *Curr. Opin. Colloid Interface Sci.* **2010,** *15* (6), 445-454.

(38) Jean, B.; Dubreuil, F.; Heux, L.; Cousin, F., Structural details of cellulose nanocrystals/polyelectrolytes multilayers probed by neutron reflectivity and AFM. *Langmuir* **2008,** *24* (7), 3452-3458.

(39) Philipse, A. P., The random contact equation and its implications for (colloidal) rods in packings, suspensions, and anisotropic powders. *Langmuir* **1996,** *12* (5), 1127-1133.

(40) Elazzouzi-Hafraoui, S.; Nishiyama, Y.; Putaux, J.-L.; Heux, L.; Dubreuil, F.; Rochas, C., The shape and size distribution of crystalline nanoparticles prepared by acid hydrolysis of native cellulose. *Biomacromolecules* **2007,** *9* (1), 57-65.

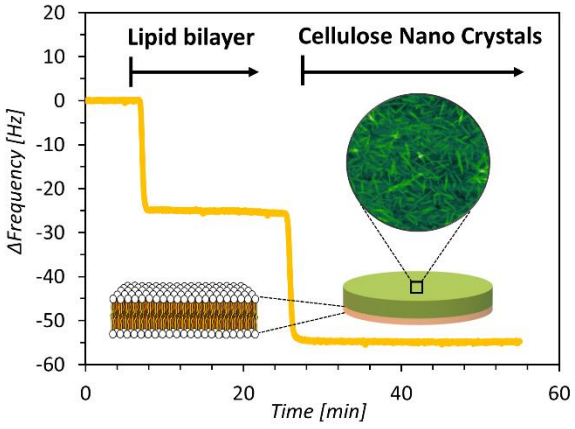
Lipid bilayer
Cellulose Nano Crystals
ΔFrequency [Hz]
Time [min]
20
10
0
-10
-20
-30
-40
-50
-60
0
20
40
60